World Academy of Science, Engineering and Technology
International Journal of Mechanical and Mechatronics Engineering
Vol:18, No:9, 2024

Hydrodynamic Characterisation of a Hydraulic Flume with Sheared Flow

Daniel Rowe, Christopher R. Vogel, Richard H. J. Willden

Abstract—This study documents the hydrodynamic characteristics of a recirculating water flume in preparation for experimental testing of horizontal axis tidal stream turbine models. An Acoustic Doppler Velocimeter (ADV) was used to measure the flow at high temporal resolution at various locations throughout the flume, enabling the spatial uniformity and turbulence flow parameters to be investigated. The mean velocity profiles exhibited high levels of spatial uniformity at the design speed of the flume, $0.6\,\mathrm{ms}^{-1}$, with variations in the three-dimensional velocity components on the order of $\pm 1\%$ at the 95% confidence level, along with a modest streamwise acceleration through the measurement domain, a target 5 m working section of the flume. A high degree of uniformity was also apparent for the turbulence intensity, with values ranging between 1-2% across the intended swept area of the turbine rotor. The integral scales of turbulence exhibited a far higher degree of variation throughout the water column, particularly in the streamwise and vertical scales. This behaviour is believed to be due to the high signal noise content leading to decorrelation in the sampling records. To achieve more realistic levels of vertical velocity shear in the flume, a simple procedure to practically generate target vertical shear profiles in open-channel flows is described. Here, we arranged a series of non-uniformly spaced parallel bars placed across the width of the flume and normal to the onset flow. By adjusting the resistance grading across the height of the working section, the downstream profiles could be modified accordingly, characterised by changes in the velocity profile power-law exponent, $1/n$. Considering the significant temporal variation in a tidal channel, the choice of the exponent denominator, $n = 6$ and $n = 9$, effectively provides an achievable range around the much-cited value of $n = 7$ observed at many tidal sites. The resulting flow profiles, which we intend to use in future turbine tests, have been characterised in detail. The results indicate non-uniform vertical shear across the survey area and reveal substantial corner flows, arising from the differential shear between the target vertical and cross-stream shear profiles throughout the measurement domain. In vertically sheared flow, the rotor-equivalent turbulence intensity ranges between 3.0-3.8% throughout the measurement domain for both bar arrangements, while the streamwise integral length scale grows from a characteristic dimension on the order of the bar width, similar to the flow downstream of a turbulence-generating grid. The experimental tests are well-defined and repeatable and serve as a reference for other researchers who wish to undertake similar investigations.

Keywords—Acoustic Doppler velocimetry, experimental hydrodynamics, open-channel flow, shear profiles, tidal stream turbines.

I. Introduction

TIDAL stream energy represents an abundant and largely unexploited source of renewable energy that can make a substantial contribution to the decarbonisation of energy systems worldwide. Despite its potential, the sector faces sizeable technical and commercial challenges as it seeks to transition from high technology readiness levels to large-scale commercial deployment. The operational capacity of tidal stream devices worldwide remains low, on $\mathcal{O}(10\text{'s})$ MW [1], a consequence of which is a scarcity of field data to inform device design. In addition, the cost and logistical complexities associated with conducting in-field test campaigns can be prohibitive, hence why carefully designed, controllable model-scale tests are often preferred.

For researchers interested in understanding the performance and response of a model-scale device, the first step is to characterise the hydrodynamic environment in which the device will be tested so that the ambient flow conditions can be quantified and the device response can be properly understood. The measurements obtained during this exercise can also help relate the facility's flow characteristics to field conditions [2]. In comparison to wind tunnels, there are relatively few publications on the characterisation of hydrodynamic research facilities. Notable examples include the work of [3]–[5], who all provided valuable insights into the capabilities and performance of their respective facilities.

Two important design criteria for a facility's hydrodynamic performance are maintaining a high spatial uniformity in flow velocity and a controlled level of low turbulence throughout the working section. Such flow conditions provide a basis for controlled experiments, allowing specific conditions to be tested and compared with analytical and numerical models. In order to replicate and evaluate the influence of in-field conditions on a device, additional mechanisms are required to generate the parameter space of interest. One such example is a graded obstruction placed normal to the onset flow to generate target vertical shear profiles. This approach was first demonstrated in wind tunnel experiments by placing a non-uniformly spaced grid of parallel rods [6] or gauze screens [7] spanning the width of the working section. In open-channel flows, several other methods of generating vertical velocity shear profiles have been reported, such as mesh panelling of variable blockage [8], active turbulence grids [9], and the strategic placement of surface roughness elements along the channel bed [10].

The objectives of this work are twofold. First, we describe the mean flow and turbulence characteristics of a recirculating water flume at the University of Oxford in preparation for experiments involving horizontal axis tidal stream turbines. Second, we apply a methodology to generate and control the vertical shear profile in the turbine's approach flow. This investigation follows the flow characterisation methodology outlined in [11] and employs an acoustic Doppler velocimeter

D. Rowe, C.R. Vogel and R.H.J. Willden are affiliated with the Department of Engineering Science, University of Oxford (e-mail: daniel.rowe@eng.ox.ac.uk).

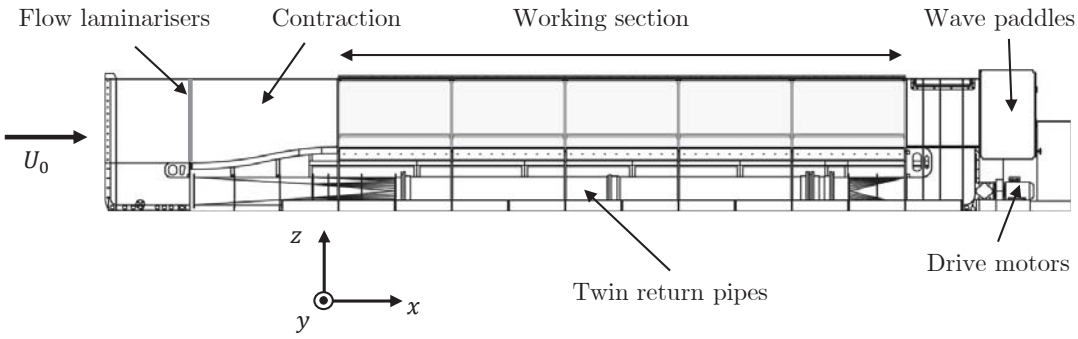

Fig. 1 Schematic of the Oxford recirculating water flume taken from [11]

(ADV) to measure the flow. The turbine to be tested has a rotor diameter of 0.6 m and is a modified version of one of two model-scale turbines tested previously at SSPA in Sweden [12].

II. Experimental Setup and Test Conditions

The University of Oxford's recirculating water flume is a combined wave and current test tank capable of delivering bulk flow speeds up to 1.0 ms^{-1}. The flume has a maximum water depth, H, of 1 m, measures 1.1 m in width, W, and has glass sides and bottom over a working length of 10 m. The flume's Cartesian coordinate system (see Fig. 1) has its origin at the centre of the cross-sectional transect at the start of the flume's working length (x = 0). Upstream of the working section are two laminarisers to straighten the flow and a horizontal and vertical contraction with arrays of guide vanes to return the flow into the working section smoothly. All experiments were run at the design speed of the flume, 0.6 ms^{-1}, and at maximum flow depth to minimise channel blockage in future turbine tests.

A 10 MHz Nortek Vectrino ADV with a downwards-looking probe was used for flow characterisation. The ADV operates by transmitting acoustic pulses into a sampling volume located 50 mm beneath the probe head. To provide sufficient back-scatter for the probe, the flume was seeded daily with kaolin clay until the signal correlation and signal-to-noise (SNR) ratio reached Nortek's recommended threshold criteria of 70% and 15 dB, respectively. Nortek cites the ADV's accuracy as $\pm 1\%$ of the measured velocity [13], defined here as a source of systematic error [14]. The instrument's nominal velocity range was configured to $\pm 0.3\,\mathrm{ms}^{-1}$ to cover the expected range of velocity fluctuations about the operating conditions. Following an assessment of the flow's temporal stability, as detailed in [11], the flow was sampled at each measurement coordinate for 300s to ensure the statistical stationarity of the sampling record. A bespoke two-dimensional (2D) linear traverse system was used to support and automate accurate positioning of the ADV.

III. Steady Flow Characterisation

This section presents the characterisation of the flume's baseline conditions in preparation for future turbine tests. The analysis comprises a range of flow metrics to quantify the spatial variation of the flume's steady flow regime.

A. Mean Velocities

Velocity signals obtained with ADVs are often contaminated by spikes caused by the aliasing of the Doppler signal. The phase-space thresholding method of Goring and Nikora [15] was used to remove anomalous results from the signals. The despiking algorithm's robustness to outliers was enhanced by incorporating the median as a location estimator and the median absolute deviation as a scale estimator, as suggested by Wahl [16]. Typically, less than 1% of the data was removed and replaced using the despiking algorithm.

Fig. 2 presents the streamwise development of the time-averaged velocity modulus[1], $\overline{U}$, in contour form across the yz plane, noting $\overline{U_0}$ is the time-averaged centreline velocity modulus at x = 5 m, where we intend to deploy the rotor in future turbine tests. Slightly higher streamwise velocities are observed in the bottom half of the water column, which is likely to be an artefact of how the flow returns to the working section via the turning vanes and the contraction section. The figure also shows an acceleration of $0.02\overline{U}$ through the streamwise length of the measurement domain when the velocities are averaged across the survey area (750 x 750 mm). At x = 7.5 m, the emergence of a shear layer along the vertical edges of the survey area becomes apparent, likely resulting from boundary layer growth and trips at the interfaces between non-co-planar glass panes, which run along the length of the flume in 1.7 m sections.

While a slight negative shear is not characteristic of velocity profiles typically observed in open-channel flows [17], there is a high degree of uniformity across the survey area, as evidenced by the narrow 95% confidence intervals for velocity variation (see Table I). Interestingly, the location of the intended rotor plane, x = 5.0 m, offers the highest level of velocity uniformity for the turbine. The variation across the survey area was calculated as $\pm 0.26\%$ at the 95% confidence level[2], $\mathrm{CI}_{0.95}$, for $\overline{U_0}$ = 0.58 ms^{-1}.

A combined experimental uncertainty of $\pm 0.007\,\mathrm{ms}^{-1}$ ($\pm 0.01\overline{U_0}$) was estimated via the root sum of squares (RSS) of the systematic, random, and sampling errors [14]. We define the random error as the 95% confidence interval for $\overline{U_0}$ from three repeated measurements and the sampling error as the

[1]The velocity modulus is deemed representative of the mean flow since the v and w velocity magnitudes $< 0.02\overline{U_0}$, and therefore negligible by comparison.

[2]The confidence interval was calculated using a two-sided t-score.

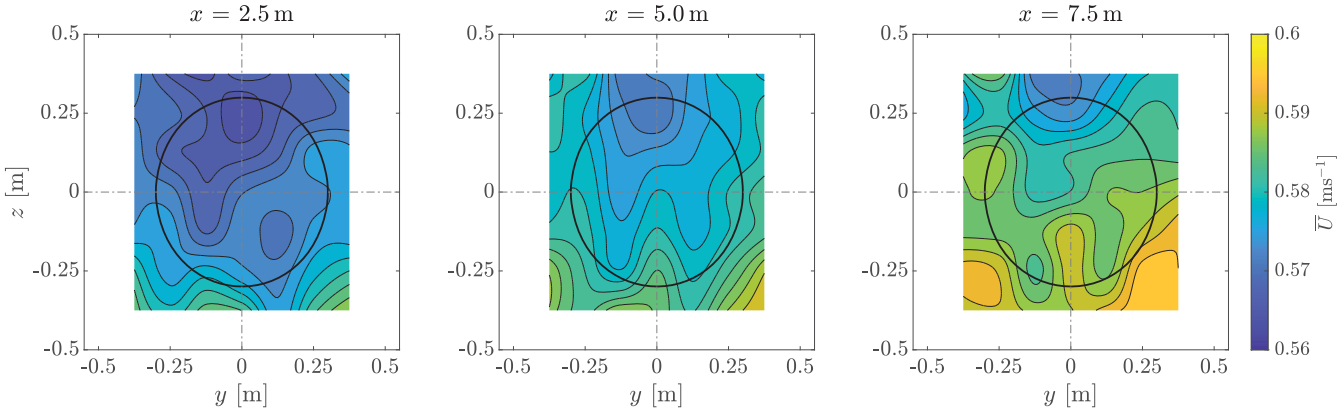

Fig. 2 Contours of $\overline{U}$ at three streamwise locations; the black circle represents the intended swept area of the turbine rotor; dataset: $\overline{U_0}$ = 0.58 ms^{-1}

uncertainty associated with the sampling of a random process. Here, an estimator variance, as defined in [18], is applied to estimate the 95% confidence bounds for the sampling error, considering any general distribution shape.

TABLE I
SUMMARY STATISTICS OF VELOCITY UNIFORMITY ACROSS INDIVIDUAL TRANSECTS OF THE FLUME

x [m]	$\langle\overline{U}\rangle/\overline{U_0}$ [-]	$\sigma(\overline{U})/\overline{U_0}$ [-]	$\mathrm{CI}_{0.95}(\overline{U})$ [%]
2.5	0.996	0.010	0.28
5.0	1.007	0.009	0.26
7.5	1.107	0.010	0.29

$\langle()\rangle$ denotes spatial averaging and σ represents the standard deviation. Dataset: $\overline{U_0}$ = 0.58 ms^{-1}.

B. Turbulence Intensities

The most commonly used metric to quantify turbulence is the turbulence intensity, I_i, which is defined with correction for noise-induced bias, $\sigma^2_{\mathrm{noise},i}$, in the i^{th} direction ($i = u, v, w$) by:

$$I_i = \sqrt{\frac{\overline{u_i'^2} - \sigma^2_{\mathrm{noise},i}}{\sum \overline{u_i}^2}}, \tag{1}$$

where the prime symbol represents a fluctuating quantity. By adopting the spectral method detailed by Voulgaris and Trowbridge [19], $\sigma^2_{\mathrm{noise},i}$ can be estimated by averaging the power spectral density (PSD) of the velocity fluctuations, S_{ii}, over a narrow band of frequencies in the tail of the spectra. Transect maps of the turbulence intensity at three streamwise locations are presented in Fig. 3, where, for brevity, we consider the magnitude of the individual directional components across three dimensions, I_{3D}. Similar to the mean velocities, a high degree of uniformity is apparent, as evidenced by the narrow range of turbulence intensities, I_{3D} = 0.9-2.1%, and low variance across the profiles, which, on average, equates to $\approx$ 2% of the spatially-averaged I_{3D} across the survey area. Higher turbulence levels associated with increased velocity shear in proximity to the sidewalls becomes apparent at x = 7.5 m, although this is unlikely to extend into the intended swept area of the rotor in future turbine tests. Combining the random and sampling errors via the RSS yields an overall uncertainty of $\pm$0.28%.

C. Probability Distributions

Establishing the best-fitting probability distributions of turbulence helps interpret experimental data by providing insights into the flow behaviour and its statistical properties. The approach here is to determine the probability distribution

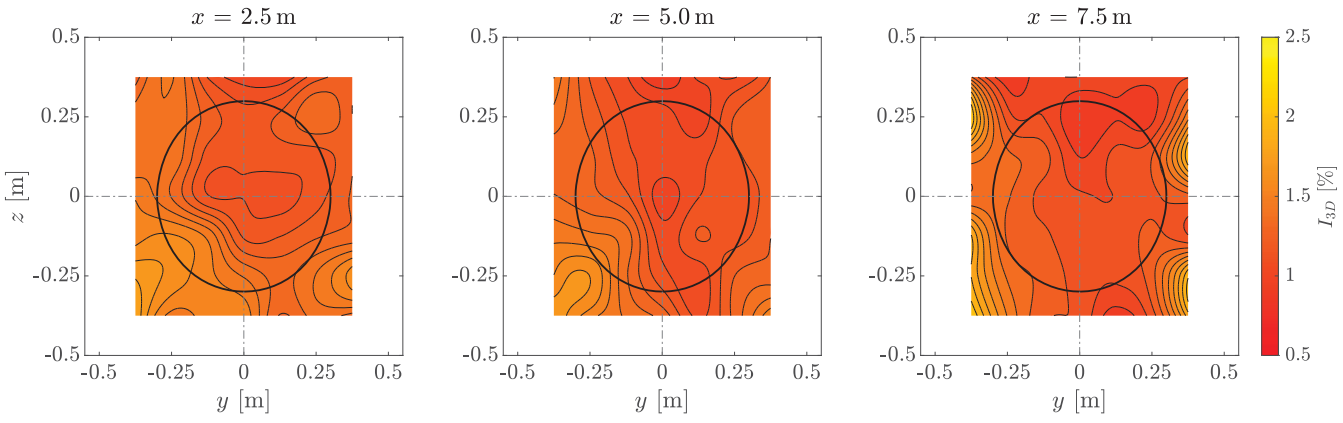

Fig. 3 Contours of I_{3D} at three streamwise locations; the black circle represents the intended swept area of the turbine rotor; dataset: $\overline{U_0}$ = 0.58 ms^{-1}

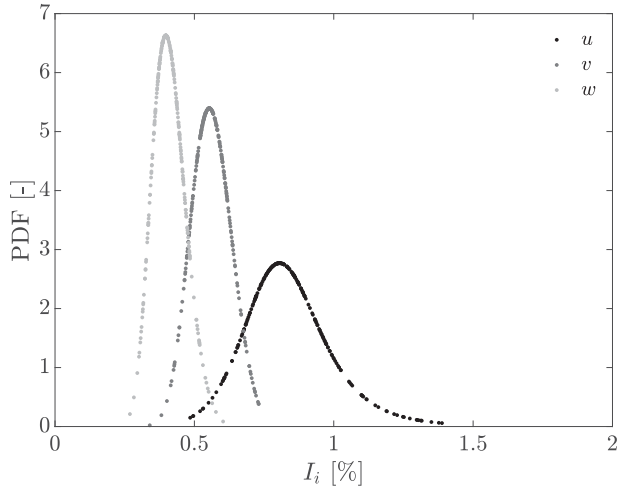

Fig. 4 Probability density function (PDF) of I_i; dataset: $\overline{U_0}$ = 0.57 ms^{-1}; measurement location $(x, y, z) = (5, 0, 0)$

that best represents the flow at the centre of the intended rotor plane. Eighteen probability distribution functions (PDFs) for binned I_i data were evaluated to identify the best-fitting model, determined by the highest-ranking log-likelihood value obtained through maximum likelihood estimation [20], [21]. For the dataset shown in Fig. 4, the log-logistic distribution best represented the I_u distribution, and the log-normal distribution ranked highest for the I_v and I_w distributions. It is worth noting that, in each case, the log-likelihood values of several distributions were comparable, implying that the highest-ranking distribution did not necessarily correspond to a statistically significant result. While the log-normal distribution features frequently in the analysis of turbulent flows, e.g. [22], the heavier tails that characterise the log-logistic distribution may better reflect the influence of the streamwise integral length scales on the mean flow [23]. The two distributions share a similar shape and are commonly applied to positively skewed datasets [24], which, in the context of an open-channel flow, appears pertinent, given the inherent skew in the velocity data, reflecting the codirectional flux of the normal Reynolds stresses [25].

Comparing the cross-stream and vertical turbulence intensities to the streamwise component provides insight into the flow anisotropy. The ratios at the centre of the intended rotor plane, $\sigma_u : \sigma_v : \sigma_w$ = 1.00 : 0.69 : 0.51, are comparable to the much-cited values of 1 : 0.71 : 0.55 from Nezu and Nakagawa [17] for 2D open-channel flows.

D. Reynolds Stresses

Reynolds' derivation of the mean-momentum equations [26] yields a symmetric second-order tensor that describes the apparent stresses resulting from the additional momentum flux in a fluctuating velocity field [27]. For incompressible flows, the shear stresses are denoted by $-\overline{u_i' u_j'}$, where $i \neq j$. Fig. 5 presents the streamwise evolution of non-dimensionalised Reynolds shear stresses as a function of depth along the vertical centre plane of the flume, along with the standard error of the mean, SE, from three repeated measurements. The profiles reveal very little change in the shear stresses with downstream distance, remaining close to zero throughout the water column. The greatest magnitudes were observed for the $-\overline{u'w'}$ stress due to shearing in the xz plane, which represents an expected result for 2D open-channel flows and is consistent with the findings of [28] and [29] at two tidal stream energy sites. The positive offset in the $-\overline{u'w'}$ stress profiles may result from a small misalignment between the ADV measurement coordinate system and the principal axes of the flow. It's important to note, however, that the impact of ADV misalignment on estimates of the Reynolds stresses is not accounted for here. The $-\overline{v'w'}$ stress consistently remains an order of magnitude smaller throughout the water column, on $\mathcal{O}(10^{-6})$ m^{2}s^{-2}, a result also reported by [30] and [31] for tidal flows.

Classical depthwise profiles of the Reynolds shear stresses in a turbulent channel typically depart from zero at the boundary and increase to a peak value within the viscous wall region before reducing linearly with wall-normal distance as the mean velocity shear asymptotes to zero [27]. The profiles presented here do not exhibit this behaviour for several reasons. First, the $\overline{U}(z)$ profiles do not resemble fully developed channel flow and instead maintain a modest negative shear through the measurement domain, which, in turn, affects the primary shear stresses [17] $-\overline{u'v'}$ and $-\overline{u'w'}$. Second, the deepest measurement coordinate, z/H = -0.385, is located 115 mm from the channel bed and thus is likely beyond the range of amplified turbulence experienced in the viscous wall region.

Analysis of the random error reveals consistently higher levels of uncertainty for the $-\overline{u'v'}$ component throughout the measurement domain, as shown by the broader $\pm 1SE$ intervals in Fig. 5. Using an estimator variance for $\overline{u_i' u_j'}$, as defined in [18], it was also possible to quantify the statistical uncertainty associated with sampling the Reynolds stresses, yielding a combined error of ± 0.008 m^{2}s^{-2} for each stress component.

E. Integral Scales

The integral scales of turbulence were calculated by applying the autocorrelation function to the velocity fluctuations at a single point in space [32]:

$$\rho_{ii}(\tau) = \frac{\overline{u_i'(t) u_i'(t+\tau)}}{{\sigma_i}^2}, \tag{2}$$

where τ represents the time lag between a signal and a delayed copy of itself, and t is a point in time. Assuming $u_i' \ll \overline{u}$, Taylor's frozen turbulence hypothesis [27], which asserts that the advection of a field of frozen turbulence is entirely due to the mean flow, can be applied, and the integral length scale, Λ_i, can be calculated by:

$$\Lambda_i = \overline{u} \int_0^\infty \rho_{ii}(\tau) d\tau, \tag{3}$$

Following the analysis of O'Neill and Nicolaides [32], the integral in (3) was evaluated using the first zero-crossing as an upper limit to τ, similar to several other studies in tidal research, e.g. [30].

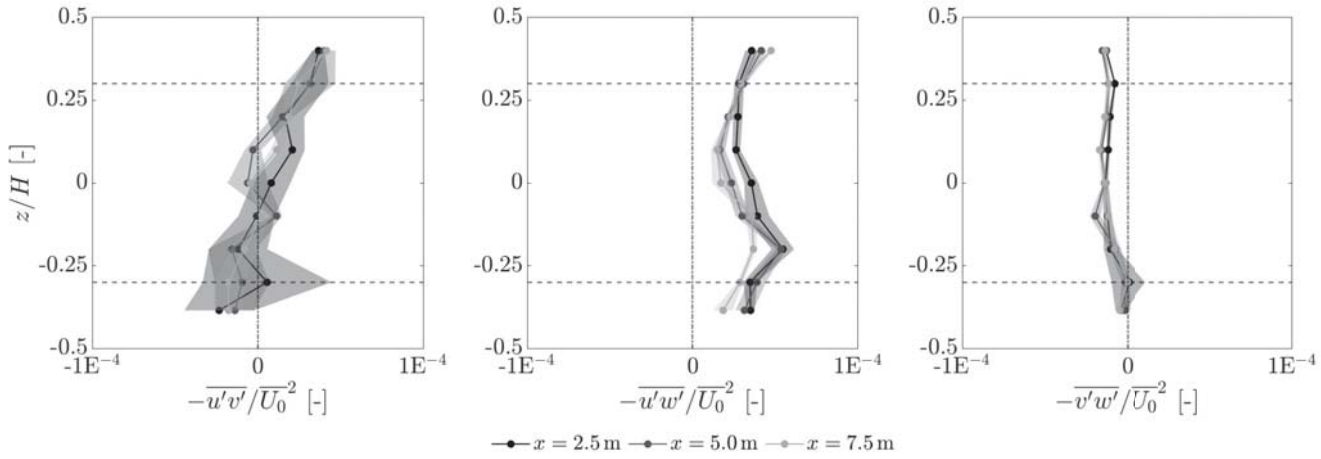

Fig. 5 Depthwise profiles of normalised Reynolds shear stresses along the flume's vertical centre plane at three streamwise locations; the random error is represented by $\pm 1SE$ (shaded areas); dataset: $\overline{U_0}$ = 0.58 ms^{-1}

Fig. 6 presents the streamwise evolution of $\Lambda_i(z)$ along the vertical centre plane of the flume, along with the SE from three repeated measurements and an empirical relationship derived by Nezu and Nakagawa [17] for 2D open-channel flows. The results reveal a higher degree of variation throughout the water column for Λ_u and Λ_w than for Λ_v, with values ranging between 0.08-1.48 m in the streamwise direction, 0.04-0.42 m in the vertical direction, and only 0.01-0.04 m in the cross-stream direction. The maxima of both $\Lambda_u(z)$ and $\Lambda_w(z)$ reside within the intended swept area of the rotor and in the lower half of the water column where the mean flow speeds are slightly higher. In contrast, the inverse relationship between Λ_v and elevation from the channel bed yields a maximum cross-stream integral length scale at $z/H = -0.385$. Determining definitive reasons for these characteristics proves challenging; however, several factors are likely to contribute to both the inter- and intra-profile variation throughout the measurement domain. First, the high signal noise content increases the likelihood of signal decorrelation and of biasing the integral scales to low values. Second, the systematic uncertainty associated with integrating the autocorrelation function compounds errors in calculations of the integral time scales.

For the uncertainty analysis, the 95% confidence intervals, based solely on the random error, are $\mathrm{CI}_{0.95}$ = $\pm$0.67 m (Λ_u), $\pm$0.01 m (Λ_v), and $\pm$0.11 m (Λ_w). The width of the intervals implies non-physical length scales and suggests that an alternative approach may be required, not only for quantifying the integral scales but also for addressing their uncertainty, particularly from velocity measurements with a high signal noise content.

F. Velocity Spectra

Estimates of the PSD provide insight into the distribution of turbulent kinetic energy across the frequency range, f, which broadly comprises three distinct regions: i) a low-frequency, energy-containing range, ii) an inertial subrange where turbulence dissipation follows a universal power law [33], and iii) a high-frequency dissipation range dominated by viscous

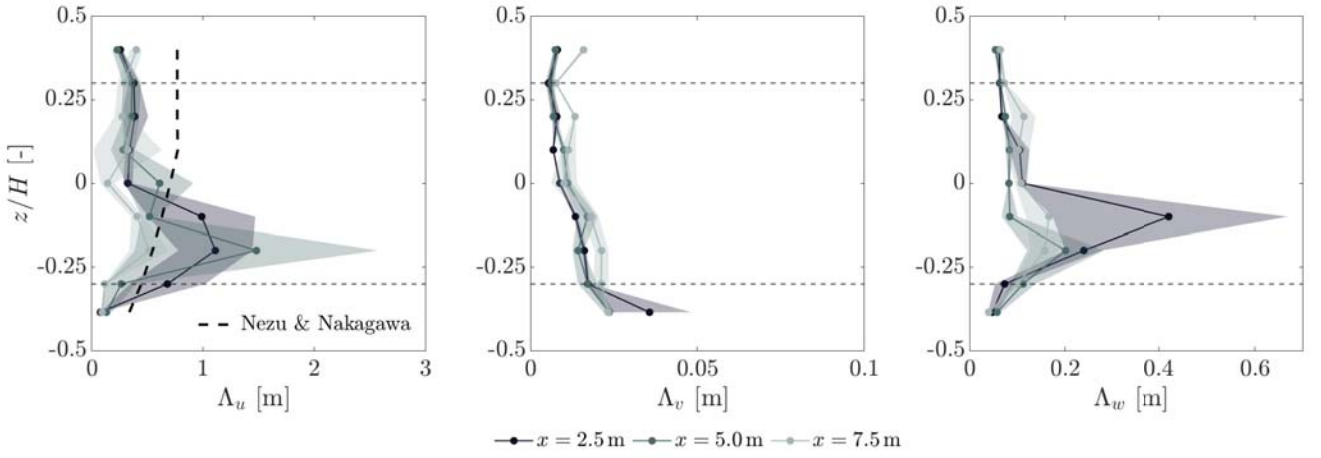

Fig. 6 Depthwise profiles of Λ_i along the flume's vertical centre plane at three streamwise locations; the random error is represented by $\pm 1SE$ (shaded areas); dataset: $\overline{U_0}$ = 0.58 ms^{-1}

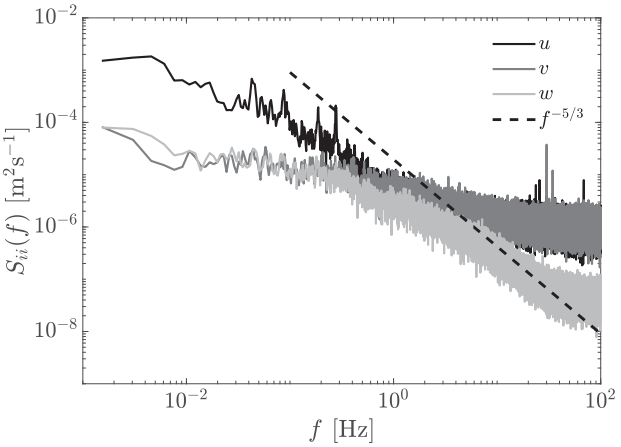

Fig. 7 Kolmogorov's $f^{-5/3}$ decay gradient (dashed) overlayed onto PSD estimates of the i^{th} component of the velocity fluctuations (greyscale), $S_{ii}(f)$; dataset: $\overline{U_0}$ = 0.57 ms^{-1}; measurement location $(x, y, z) = (5, 0, 0)$

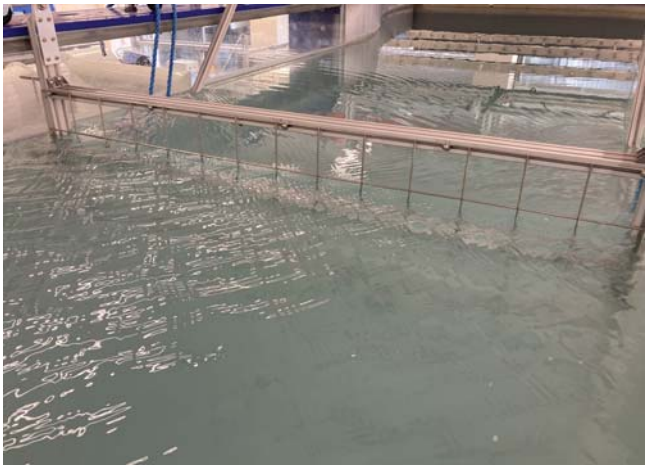

Fig. 8 Photo of the welded mesh panel affixed to the downstream face of the aluminium frame; the shallowest submerged horizontal bars can be seen just beneath the free surface

effects. The exact frequencies that bound each region are not always apparent, as indicated in Fig. 7. The dissipation range, for instance, is masked by signal noise, which corresponds to spectral flattening at higher frequencies, particularly in the streamwise and cross-stream components. The figure also reveals at least an order-of-magnitude difference in spectral energy between the streamwise and orthogonal components at the lower end of the frequency range. This is an expected result for controlled open-channel flow conditions and implies the flow's tendency towards one-dimensionality. The cross-stream velocity spectra's divergence from the $f^{-5/3}$ decay gradient suggests the signal may be disproportionately contaminated by noise in low turbulence conditions, noting the vertical velocity spectrum is much less sensitive to noise due to the ADV beam geometry [19].

IV. Shear Profile Generation

The shape of a tidal channel's vertical shear profile is a function of several contributing factors, such as the bed roughness, the point in the tidal cycle, and the prevailing met-ocean conditions. As a result, the inter- and intra-site variation of vertical shear can be extensive, leading to a complex onset flow profile, varying continuously throughout the tidal cycle. The velocity profile at many sites is conveniently approximated by a power-law model [34]:

$$\frac{\overline{u}(z)}{\overline{U_0}} = \left(\frac{z^*}{H}\right)^{1/n}, \tag{4}$$

where z^* $(= z + 0.5)$ reflects the elevation from the channel bed, and $1/n$ is the power-law exponent characterising the level of vertical shear in the profile. Lewis et al. [34] found that n = 7 provided a reasonable approximation of the mean velocity profiles across potential tidal stream energy sites in the Irish Sea. The present study makes use of this finding to guide the design of a vertical shear profile generation system.

A. Methodology

For the production of vertical shear profiles represented by the power-law model, the authors applied an empirical approach to the method of Cowdrey [35]. Similar to the approach taken by Owen and Zienkiewicz [6], Cowdrey proposed a simple mathematical treatment to arrange a series of non-uniformly spaced parallel circular rods across the width of the working section, placed normal to the onset flow. By adjusting the resistance grading throughout the height of the working section, the downstream velocity profiles could be modified accordingly, characterised by changes in n. For the present study, a flexible and modular frame comprising standard aluminium extrusions was developed, allowing a range of flow-resisting geometries to be investigated. The yz plane of the frame, denoted by the subscript F, was positioned at x_F = 1.5 m. Rather than using circular rods, we arranged a series of square bars (cross section 20×20 mm) horizontally on the upstream face of the frame and affixed a welded mesh panel (mesh size = 0.075 m, gauge = 0.003 m) on the downstream face, as shown in Fig. 8. The mesh panel's purpose was to enhance flow mixing and break up coherent structures shed from the bars.

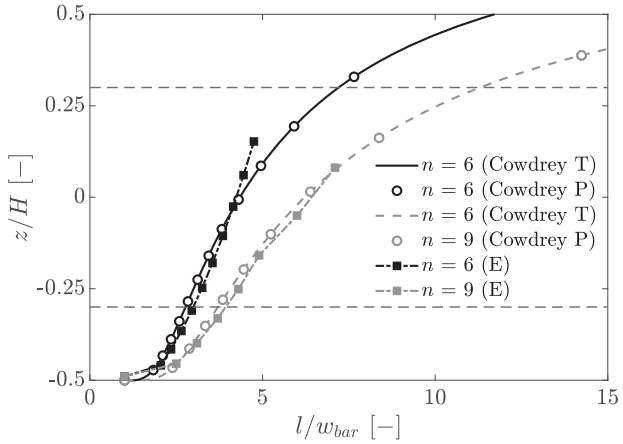

Fig. 9 Bar spacing configuration curves for two power-law velocity distributions, where l represents the centre-to-centre bar spacing; a practical (P) implementation of Cowdrey's theory (T) are overlaid onto experimental results (E)

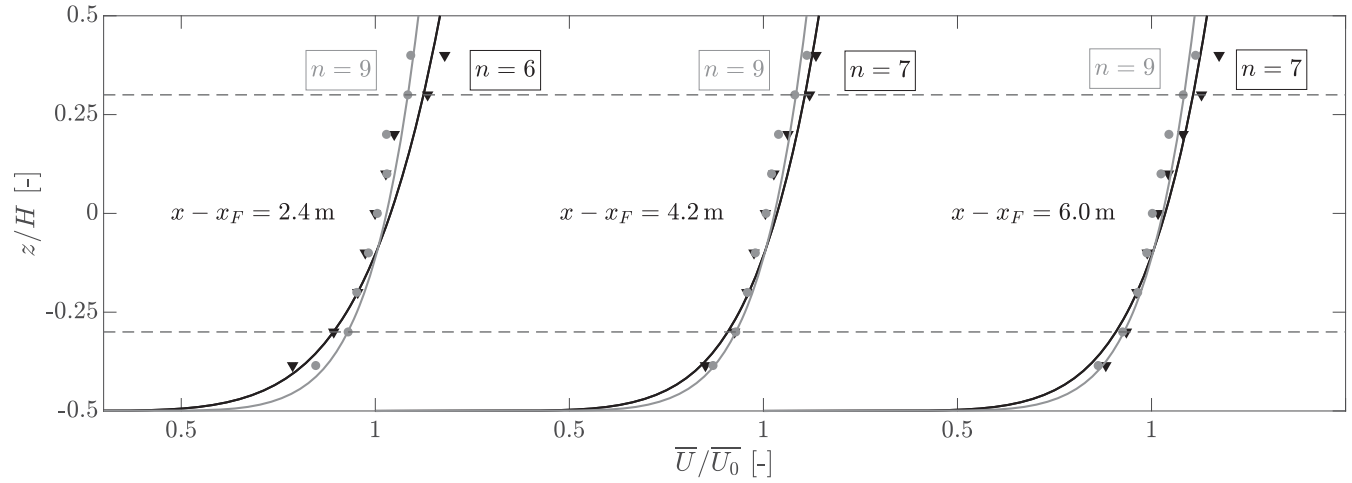

Fig. 10 Depthwise profiles of $\overline{U}/\overline{U_0}$ at three streamwise locations along the vertical centre plane of the flume; the measured velocities (symbols) are superimposed onto best fit power-law velocity profiles (solid lines); the intended swept area of the turbine rotor is also shown (dashed lines); $\overline{U_0}$ = 0.61 ms^{-1}

To demonstrate the application of this approach, two vertical shear profiles with exponent denominators, n = 6 and n = 9, were generated. This choice of exponent denominators effectively establishes an achievable range around the much-cited value of n = 7, capturing in part the considerable variation throughout the tidal cycle. For both exponent denominators, the initial positioning of the bars was based on Cowdrey's theory; however, careful adjustments in the relative spacing between bars were necessary to minimise the root-mean-square error between the measured streamwise velocities throughout the water column and the theoretical distribution corresponding to the target (integer) exponent denominator from (4). The error criterion was set to $\leq 0.03\,\mathrm{ms}^{-1}$. The error was calculated at the design speed of the flume along the flume's vertical centre at the intended rotor plane, which, for turbine experiments behind the frame, is located four rotor diameters downstream of the frame, $x-x_F$ = 2.4 m. Fig. 9 shows a close agreement in the bottom two-thirds of the water column between the final bar positions and those predicted theoretically based on Cowdrey's model, noting no bars were placed at $z/H > 0.15$. The ratio of open area to channel area, θ, of each bar arrangement was calculated as $\theta(n = 6) = 0.76$ and $\theta(n = 9) = 0.81$.

B. Application

Fig. 10 presents depthwise profiles of $\overline{U}$ normalised on $\overline{U_0}$ along the vertical centre plane of the flume at three streamwise locations, noting $\overline{U_0}$ was calculated at $x - x_F = 2.4\,\mathrm{m}$. Theoretical velocity distributions, represented by the power-law model, are included as a reference. In contrast with the vertical shear profile characterised by $n = 9$ at the intended rotor plane, the corresponding profile for $n = 6$ is not maintained through the measurement domain, as indicated by the small reduction in vertical velocity shear, $n = 6 \rightarrow 7$, that occurs as the profile develops between $x - x_F = 2.4\,\mathrm{m}$ and $4.2\,\mathrm{m}$. No change in the exponent denominators were observed across three repeated measurements.

For a more complete view of the velocity field in sheared flow, Fig. 11 presents 2D contour plots of the velocity modulus for n = 6 at three streamwise locations. The results reveal a non-uniform distribution of vertical shear across the width of the survey area. This non-uniformity is attributed to the differential shear between the cross-stream and target vertical shear profiles, resulting in turbulence anisotropy and the development of substantial corner flows through the measurement domain. We note that the presence of the discrete aluminium apparatus additionally influences the development of the observed corner flows. Away from the vertical centre plane of the channel, the vertical shear increases, reaching a maximum flow speed at $y = \pm 0.375\,\mathrm{m}$, where the depthwise profile throughout the water column can be characterised by n = 4. As the flow convects downstream, the profiles remain broadly symmetrical about $y = 0$; however, the intended swept area of the rotor becomes increasingly penetrated by two corner flows as the isovels in the lower half of the water column progressively bulge towards the core of the channel along the corner bisectors. In narrow open-channel flows, where the aspect ratio $W/H \leq 5$, the core flow is particularly susceptible to the lateral transfer of near-wall momentum [17], despite the secondary currents being at least one order of magnitude smaller than the dominant streamwise velocity. In contrast to the steady flow regime described in Section III-A, the flow exhibits a modest deceleration of $0.01\overline{U}$ through the measurement domain when the velocities are spatially averaged across the survey area.

When comparing the velocity fields characterised by the power-law exponent denominators n = 6 and n = 9 (not shown), the impact of a different θ imposed by the bar arrangement appears modest; however, differences in the global flow metrics should be accounted for when analysing turbine performance metrics. Here, we consider a spatially-averaged velocity across the survey area at the intended rotor plane, which yields a relative difference between the datasets of 1.5%, noting the n = 9 test setup results in slightly higher approach flow speed. In the context of energy flux, a relative increase of 1.5% in the rotor-equivalent flow speed corresponds to a nominal increase in energy flux

of 4.6%, which may or may not result in a change in turbine power depending on how it is operated, local blockage effects, and drivetrain losses etc.

The time-averaged 2D contours of I_{3D} for $n = 6$ at three streamwise locations are presented in Fig. 12. As with the velocity modulus, the figure reveals significant vertical and lateral variation, with the highest turbulence intensities confined to the bottom corners of the channel. At $z/H = 0.375$, the turbulence at each streamwise location is slightly elevated (I_{3D} = 1.6-2.0%) relative to the steady flow condition, which we attribute to the absence of horizontal bars at $z/H > 0.15$. Fig. 12 also provides insight into the transient nature of turbulence as it decays beyond the production region, most evidently along the flume's centreline. In this context, we note a progressive reduction in the range, variance, and anisotropy of the turbulence intensities (σ_u : σ_v : σ_w) through the measurement domain, resulting in a modest reduction of the vertical velocity shear through the water column, as highlighted previously in Fig. 10. The rotor-equivalent turbulence intensity ranges between I_{3D} = 3.0-3.8% throughout the measurement domain for both bar arrangements.

Fig. 13 presents the streamwise evolution of $\Lambda_u(z)$ in sheared flow (target exponent denominator $n = 6$) along the vertical centre plane of the flume, along with the SE from three repeated measurements. For measurements at depths of $z/H > 0.2$, there is a comparable level of variation as observed in the steady flow profiles, noting that the largest scales remain confined to a region where the turbulence intensity is relatively low ($\leq 2\%$). In addition, the results suggest some length scales towards the top of the water column exceed the channel height - a scenario that seems unlikely, raising further concerns about the suitability of this approach to this metric in low turbulence conditions. In contrast, the degree of variation for measurements obtained directly behind the horizontal bars, where $z/H < 0.15$, is considerably lower, yielding a 95% confidence interval, based solely on the random error, of $\mathrm{CI}_{0.95} = \pm 0.05$ m. The contrast in random error across the profile highlights the sensitivity of the autocorrelation function to the amount of signal noise and turbulence in the measured flow, which can be related to the positioning of the bars in the water column. Towards the top of the water column, where no bars are present, the turbulence is low, and the signal noise constitutes a relatively large proportion ($> 50\%$) of the measured variance, yielding disproportionately wide confidence intervals in the random error. Conversely, in the bottom two-thirds of the water column, where turbulence is higher, the flow-related content of the signal dominates over Doppler noise ($< 10\%$), resulting in much narrower confidence intervals. As the turbulence decays downstream, we observe a corresponding growth in the length scales, a trend also observed in the flow downstream of a turbulence-generating grid. The growth of length scales starting from a characteristic dimension on $\mathcal{O}(w_{\mathrm{bar}})$ just downstream of a grid, has been well documented in the literature [36].

V. Conclusions

The mean flow and turbulence properties of a recirculating water flume at the University of Oxford have been characterised. The initial phase of the investigation focused on the flume's ambient flow conditions, for which the authors adhered to a rigorous methodology detailed in [11], which accounts for biases within the test setup and measurement uncertainty.

The time-averaged velocity profiles exhibited high levels of spatial uniformity, with deviations in flow speed $< 1\%$ at the 95% confidence level, along with a modest streamwise acceleration through the measurement domain. The emergence of a shear layer along both vertical edges of the survey area was also observed, although it is unlikely that they will penetrate the swept area of the rotor in future turbine tests.

A high degree of uniformity was also apparent for the turbulence intensities throughout the measurement domain, with values ranging between 1-2% across the intended swept area of the rotor. Slightly higher turbulence intensities were measured close to the edges of the survey area. The flow anisotropy, defined by the ratios of the turbulence intensities, closely aligned with observations from idealised open-channel flow experiments, and the probability distributions that best represented binned turbulence intensity data were the log-logistic (I_u) and the log-normal (I_v, I_w) distributions.

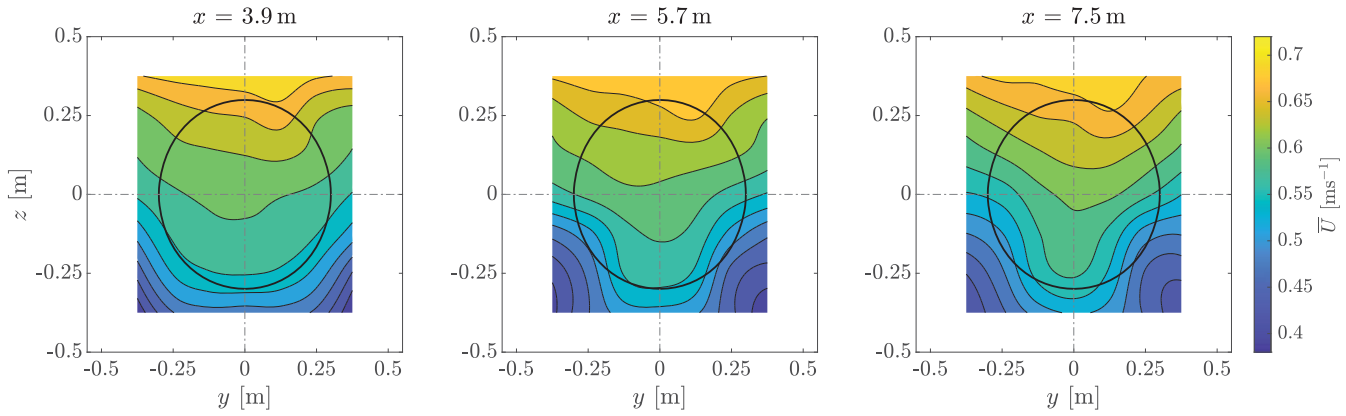

Fig. 11 Contours of $\overline{U}$ in sheared flow (target $n = 6$) at three streamwise locations; the black circle represents the intended swept area of the turbine rotor; dataset: $\overline{U_0} = 0.61$ ms^{-1}

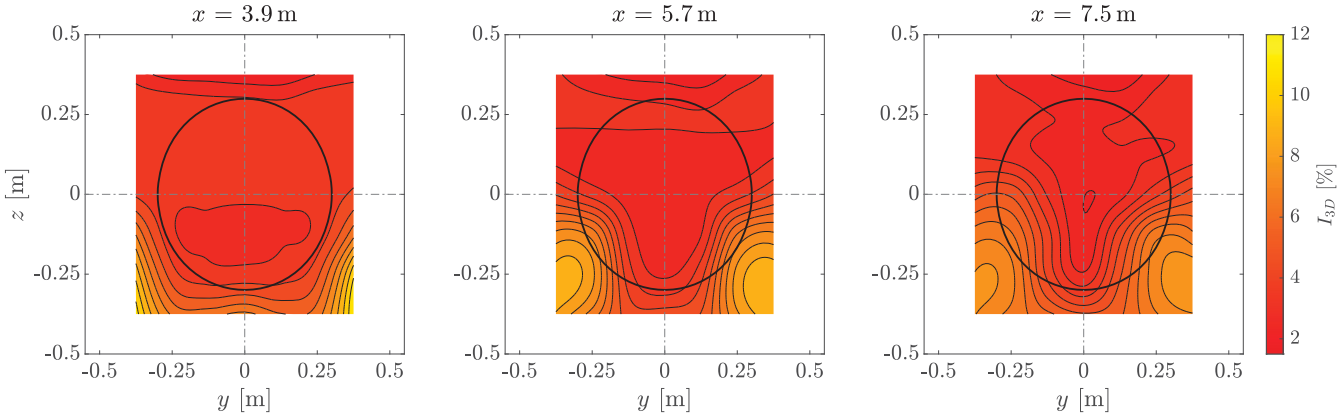

Fig. 12 Contours of I_{3D} in sheared flow (target n = 6) at three streamwise locations; the black circle represents the intended swept area of the turbine rotor; dataset: $\overline{U_0}$ = 0.61 ms^{-1}

Depthwise profiles of the Reynolds shear stresses exhibited very little change throughout the water column, indicating that the measurement coordinates were likely beyond the influence of boundary-induced shear stresses. The largest magnitudes were observed for the $-\overline{u'w'}$ component, representing an expected result for 2D open-channel flows.

The integral scales of turbulence exhibited a high degree of variation across repeated measurements, particularly in the streamwise and vertical scales. This behaviour is believed to be due to the high signal noise content, leading to decorrelation in the sampling records. The wide 95% confidence intervals imply non-physical length scales and suggest that an alternative approach may be required, not only for quantifying the integral scales but also for addressing their uncertainty, particularly from velocity measurements with a high signal noise content.

There was at least one order-of-magnitude difference in the spectral energy between the horizontal and orthogonal components of velocity fluctuations at the lower end of the frequency range. This is an expected result for controlled open-channel flow conditions and is consistent with the flow's tendency towards one-dimensionality.

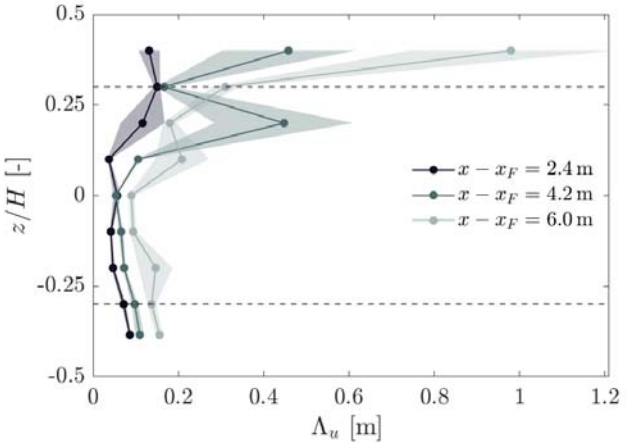

Fig. 13 Depthwise profiles of Λ_u along the flume's vertical centre plane at three streamwise locations in sheared flow (target n = 6); the random error is represented by $\pm 1SE$ (shaded areas); dataset: $\overline{U_0}$ = 0.61 ms^{-1}

In the second phase of the investigation, the focus shifted to the practical application of a methodology for generating vertical velocity shear in the flume, the target profiles of which are represented by a power-law model. Here, the authors applied an empirical approach to the method of Cowdrey to define a graded resistance across the width of the working section to generate two target vertical shear profiles characterised by the denominator of the power-law exponent. After applying a practical criterion to finalise the geometry of the graded resistance for each target profile, the bar arrangement aligned closely with the theoretical predictions from Cowdrey's model.

The results reveal non-uniform vertical shear across the survey area and the presence of substantial corner flows, attributed to the differential shear between the target vertical and cross-stream shear profiles. Away from the vertical centre plane of the channel, the vertical shear increases, reaching a maximum flow speed at $y = \pm 0.375$ m, where the depthwise profile throughout the water column can be characterised by n = 4. The results also show that, for the $n = 6$ bar arrangement, there is a modest reduction in vertical velocity shear along the vertical centre plane of the channel with downstream distance. At $x - x_F = 6.0$ m, the vertical velocity profile can be characterised by $n = 7$.

Time-averaged contours of the turbulence intensity confirm the significant vertical and lateral variation across the survey area, with the highest turbulence intensities confined to the bottom corners of the survey area. As the vertical velocity shear gradually reduces with downstream distance, the turbulence decays across the survey area, and we observe a corresponding growth in the streamwise integral length scales, similar to the flow downstream of a turbulence-generating grid. The streamwise profiles of Λ_u along the vertical centre plane of the channel also reveal contrasting levels of random error throughout the water column, highlighting the sensitivity of the autocorrelation function to the amount of signal noise and turbulence in the measured flow, which can be related to the positioning of the bars in the water column.

ACKNOWLEDGMENT

This research was funded in part by DR's EPSRC studentship (grant no. EP/S023801/1), CRV's UKRI Future Leaders Fellowship (grant no. MR/V02504X/1), RHJW's EPSRC Advanced Fellowship (grant no. EP/R007322/1), and the EPSRC Supergen ORE Hub (grant no. EP/S000747/1).

REFERENCES

[1] D. Coles, A. Angeloudis, D. Greaves, G. Hastie, M. Lewis, L. Mackie, J. McNaughton, J. Miles, S. P. Neill, M. D. Piggott, D. Risch, B. Scott, C. Spalding, T. Stallard, P. Thies, S. Walker, D. White, R. H. J. Willden, and B. Williamson, "A review of the UK and British Channel Islands practical tidal stream resource," *Proceedings of the Royal Society A: Mathematical, Physical and Engineering Sciences*, vol. 477, no. 2255, 2021.

[2] D. R. Noble, S. Draycott, S. Ordonez Sanchez, K. Porter, C. Johnstone, S. Finch, F. Judge, C. Desmond, B. Santos Varela, J. Lopez Mendia, D. Darbinyan, F. Khalid, L. Johanning, M. Le Boulluec, and A. Schaap, "Test recommendations and gap analysis report," MaRINET2, Technical Report, 2018.

[3] J. Park, J. M. Cutbirth, and W. H. Brewer, "Hydrodynamic performance of the large cavitation channel (LCC)," in *Proceedings of the ASME/JSME 2003 4th Joint Fluids Summer Engineering Conference, Vol. 2: Symposia, Parts A, B, and C*, Hawaii, USA, 2003, pp. 87–100.

[4] T. Mori, K. Naganuma, R. Kimoto, R. Yakushiji, and S. Nagaya, "Hydrodynamic and hydroacoustic characteristics of the flow noise simulator," in *Proceedings of the ASME/JSME 2007 5th Joint Fluids Engineering Conference, Vol. 2*, California, USA, 2007, pp. 121–127.

[5] D. R. J. Sutherland, D. R. Noble, J. Steynor, T. Davey, and T. Bruce, "Characterisation of current and turbulence in the FloWave Ocean Energy Research Facility," *Ocean Engineering*, vol. 139, pp. 103–115, 2017.

[6] P. R. Owen and H. K. Zienkiewicz, "The production of uniform shear flow in a wind tunnel," *Journal of Fluid Mechanics*, vol. 2, no. 6, p. 521–531, 1957.

[7] J. W. Elder, "Steady flow through non-uniform gauzes of arbitrary shape," *Journal of Fluid Mechanics*, vol. 5, pp. 355 – 368, 1959.

[8] M. Islam, D. Spencer, P. Herrington, D. Walker, H. Moideen, and Y. C. Park, "Sheared current generation in flume tank for experimental research," in *Proceedings of the International Conference on Offshore Mechanics and Arctic Engineering*, vol. 1, Nantes, France, 2013, pp. 1–12.

[9] A. Vinod, C. Han, and A. Banerjee, "Tidal turbine performance and near-wake characteristics in a sheared turbulent inflow," *Renewable Energy*, vol. 175, pp. 840–852, 2021.

[10] A. Robert, A. G. Roy, and B De Serres, "Changes in velocity profiles at roughness transitions in coarse grained channels," *Sedimentology*, vol. 39, pp. 725–735, 1992.

[11] D. Rowe, C. R. Vogel, and R. H. J. Willden, "Experimental methodology for hydrodynamic characterisation of a hydraulic flume," 2023, unpublished Manuscript.

[12] J. McNaughton, S. Ettema, F. Zilic de Arcos, C. R. Vogel, and R. H. J. Willden, "An experimental investigation of the influence of inter-turbine spacing on the loads and performance of a co-planar tidal turbine fence," *Journal of Fluids and Structures*, vol. 118, p. 103844, 2023.

[13] Nortek, "The comprehensive manual for velocimeters," Manual, Norway, 2018, accessed: 2021-07-10. [Online]. Available: https://support.nortekgroup.com/hc/en-us/article_attachments/4551609336220

[14] H. W. Coleman and W. Glenn Steele Jr., *Experimentation, Validation, and Uncertainty Analysis for Engineers*. United States of America: John Wiley & Sons, Inc., 2009.

[15] D. G. Goring and V. I. Nikora, "Despiking acoustic Doppler velocimeter data," *Journal of Hydraulic Engineering*, vol. 128, no. 1, pp. 117–126, 2002.

[16] T. L. Wahl, "Discussion of "Despiking acoustic Doppler velocimeter data" by Derek G. Goring and Vladimir I. Nikora," *Journal of Hydraulic Engineering*, vol. 129, no. 6, pp. 484–487, 2003.

[17] I. Nezu and H. Nakagawa, *Turbulence in Open-Channel Flows*. Netherlands: A.A. Balkema, 1993.

[18] L. H. Benedict and R. D. Gould, "Towards better uncertainty estimates for turbulence statistics," *Experiments in Fluids*, vol. 22, pp. 129–136, 1996. [Online]. Available: https://doi.org/10.1007/s003480050030

[19] G. Voulgaris and J. H. Trowbridge, "Evaluation of the acoustic Doppler velocimeter (ADV) for turbulence measurements," *Journal of Atmospheric and Oceanic Technology*, vol. 15, pp. 272–289, 1998.

[20] F. de Castro, "fitmethis version 1.6.1," 2021, retrieved: 2023-06-06. [Online]. Available: https://uk.mathworks.com/matlabcentral/fileexchange/40167-fitmethis

[21] R. V. Hogg, J. W. McKean, and A. T. Craig, *Introduction to Mathematical Statistics*. United States of America: Prentice Hall, 2005.

[22] K. Christakos, J. Reuder, and B. Furevik, "Experimental characterization of the marine atmospheric boundary layer in the Havsul area, Norway," *Energy Procedia*, vol. 35, pp. 121–127, 2013, deepWind'2013 – Selected papers from 10th Deep Sea Offshore Wind R&D Conference, Trondheim, Norway.

[23] O. P. Folorunso, "Probability distribution of turbulent velocity fluctuations in a patchy vegetated open channel," *Journal of Civil & Environmental Engineering*, vol. 7, 2017.

[24] M. Z. Raqab, S. A. Al-Awadhi, and D. Kundu, "Discriminating among Weibull, log-normal, and log-logistic distributions," *Communications in Statistics - Simulation and Computation*, vol. 47, no. 5, pp. 1397–1419, 2018.

[25] P. Hanmaiahgari, V. Roussinova, and R. Balachandar, "Turbulence characteristics of flow in an open channel with temporally varying mobile bedforms," *Journal of Hydrology and Hydromechanics*, vol. 65, 2017.

[26] O. Reynolds, "IV. On the dynamical theory of incompressible viscous fluids and the determination of the criterion," *Philosophical Transactions of the Royal Society of London. (A.)*, vol. 186, pp. 123–164, 1895.

[27] S. Pope, *Turbulent Flows*. United States of America: Cambridge University Press, 2014.

[28] I. A. Milne, R. N. Sharma, and R. G. J. Flay, "The structure of turbulence in a rapid tidal flow," *Proceedings of the Royal Society A: Mathematical, Physical and Engineering Sciences*, vol. 473, 2017.

[29] M. Togneri and I. Masters, "Comparison of marine turbulence characteristics for some potential turbine installation sites," in *Proceedings of the 4th Internation Conference on Ocean Energy*, Dublin, Ireland, 2012.

[30] M. Thiébaut, J.-F. Filipot, C. Maisondieu, D. Guillaume, C. Jochum, L. Kilcher, and G. Sylvain, "Characterization of the vertical evolution of the three-dimensional turbulence for fatigue design of tidal turbines," *Philosophical Transactions of The Royal Society A Mathematical Physical and Engineering Sciences*, vol. 378, p. 20190495, 2020.

[31] R. K. Walter, N. J. Nidzieko, and S. G. Monismith, "Similarity scaling of turbulence spectra and cospectra in a shallow tidal flow," *Journal of Geophysical Research: Oceans*, vol. 116, no. C10, 2011.

[32] P. L. O'Neill, D. Nicolaides, D. R. Honnery, and J. Soria, "Autocorrelation functions and the determination of integral length with reference to experimental and numerical data," in *Proceedings of the 15th Australasian Fluid Mechanics Conference*, Sydney, Australia, 2004.

[33] A. N. Kolmogorov, "The local structure of turbulence in incompressible viscous fluid for very large Reynolds numbers," *Proceedings: Mathematical and Physical Sciences*, vol. 434, no. 1890, pp. 9–13, 1991.

[34] M. Lewis, S. P. Neill, P. Robins, M. R. Hashemi, and S. Ward, "Characteristics of the velocity profile at tidal-stream energy sites," *Renewable Energy*, vol. 114, pp. 258–272, 2017.

[35] C. F. Cowdrey, "A simple method for the design of wind-tunnel velocity-profile grids," National Physical Laboratory, Teddington, UK, Tech. Rep. Aero Note 1055, 1967.

[36] P. E. Roach, "The generation of nearly isotropic turbulence by means of grids," *International Journal of Heat and Fluid Flow*, vol. 8, no. 2, pp. 82–92, 1987.